5. R. O. Pepin, *Icarus* **92**, 2 (1991).
6. R. O. Pepin, *Earth Planet. Sci. Lett.* **252**, 1 (2006).
7. S. Sasaki, *Icarus* **91**, 29 (1991).
8. T. Owen, A. Bar-Nun, I. Kleinfeld, *Nature* **358**, 43 (1992).
9. M. Trieloff, J. Kunz, C. J. Allegre, *Earth Planet. Sci. Lett.* **200**, 297 (2002).
10. C. J. Ballentine, B. Marty, B. Sherwood Lollar, M. Cassidy, *Nature* **433**, 33 (2005).
11. B. Marty *et al.*, *Science* **319**, 75 (2008).
12. G. Notesco, D. Laufer, A. Bar-Nun, T. Owen, *Icarus* **142**, 298 (1999).
13. A. Morbidelli *et al.*, *Meteorit. Planet. Sci.* **35**, 1309 (2000).
14. C. Allègre, T. Staudacher, P. Sarda, *Earth Planet. Sci. Lett.* **81**, 127 (1987).
15. C. L. Harper Jr., S. B. Jacobsen, *Science* **273**, 1814 (1996).
16. G. Holland, C. J. Ballentine, *Nature* **441**, 186 (2006).
17. C. J. Ballentine, G. Holland, *Philos. Trans. R. Soc. London Ser. A* **366**, 4183 (2008).
18. T. Staudacher, *Nature* **325**, 605 (1987).
19. M. W. Caffee *et al.*, *Science* **285**, 2115 (1999).
20. Materials and methods are available as supporting material on *Science* Online.
21. R. O. Pepin, D. Porcelli, *Earth Planet. Sci. Lett.* **250**, 470 (2006).
22. M. Moreira, J. Kunz, C. Allègre, *Science* **279**, 1178 (1998).
23. D. Porcelli, G. J. Wasserburg, *Geochim. Cosmochim. Acta* **59**, 4921 (1995).
24. P. Signer, H. E. Suess, *Earth Science and Meteoritics*, J. Geiss, E. D. Goldberg, Eds. (North-Holland, Amsterdam, 1963).
25. T. M. Donahue, *Icarus* **66**, 195 (1986).
26. M. Touboul, T. Kleine, B. Bourdon, H. Palme, R. Wieler, *Nature* **450**, 1206 (2007).
27. T. J. Ahrens, *Annu. Rev. Earth Planet. Sci.* **21**, 525 (1993).
28. H. Genda, Y. Abe, *Nature* **433**, 842 (2005).
29. A. Bar-Nun, I. Kleinfeld, E. Kochavi, *Phys. Rev. B* **38**, 7749 (1988).
30. N. Dauphas, *Icarus* **165**, 326 (2003).
31. R. O. Pepin, *Space Sci. Rev.* **106**, 211 (2003).
32. D. York, *Earth Planet. Sci. Lett.* **5**, 320 (1969).
33. We thank Oxy and Amerada Hess corporations for permission to sample the Bravo Dome Field. We thank D. Blagburn and B. Clementson for laboratory support and R. Pepin for discussions on the manuscript. This work was funded by UK Natural Environment Research Council.

Supporting Online Material
www.sciencemag.org/cgi/content/full/326/5959/1522/DC1
Materials and Methods
Figs. S1 to S5
Tables S1 to S4
References

22 July 2009; accepted 23 October 2009
10.1126/science.1179518

Evolution of Organic Aerosols in the Atmosphere

J. L. Jimenez,[1]* M. R. Canagaratna,[2] N. M. Donahue,[3] A. S. H. Prevot,[4]* Q. Zhang,[5,6] J. H. Kroll,[2,7] P. F. DeCarlo,[1,4,8] J. D. Allan,[9,10] H. Coe,[9] N. L. Ng,[2] A. C. Aiken,[1]† K. S. Docherty,[1] I. M. Ulbrich,[1] A. P. Grieshop,[3]‡ A. L. Robinson,[3] J. Duplissy,[4]§ J. D. Smith,[11] K. R. Wilson,[11] V. A. Lanz,[4,12] C. Hueglin,[12] Y. L. Sun,[5,6] J. Tian,[5] A. Laaksonen,[13,14] T. Raatikainen,[13,14] J. Rautiainen,[13] P. Vaattovaara,[13] M. Ehn,[15] M. Kulmala,[15,16] J. M. Tomlinson,[17]‖ D. R. Collins,[17] M. J. Cubison,[1] E. J. Dunlea,[1]¶ J. A. Huffman,[1]# T. B. Onasch,[2] M. R. Alfarra,[4,9,10] P. I. Williams,[9,10] K. Bower,[9] Y. Kondo,[18] J. Schneider,[19] F. Drewnick,[5,19] S. Borrmann,[19,20] S. Weimer,[4,5,21] K. Demerjian,[5] D. Salcedo,[22] L. Cottrell,[23]†† R. Griffin,[23,24] A. Takami,[25] T. Miyoshi,[25]‡‡ S. Hatakeyama,[25]§§ A. Shimono,[26] J. Y Sun,[27] Y. M. Zhang,[27] K. Dzepina,[1,28]¶¶ J. R. Kimmel,[1,2,29] D. Sueper,[1,2] J. T. Jayne,[2] S. C. Herndon,[2]‖‖ A. M. Trimborn,[2] L. R. Williams,[2] E. C. Wood,[2] A. M. Middlebrook,[30] C. E. Kolb,[2] U. Baltensperger,[4] D. R. Worsnop[2,13,14,15]

Organic aerosol (OA) particles affect climate forcing and human health, but their sources and evolution remain poorly characterized. We present a unifying model framework describing the atmospheric evolution of OA that is constrained by high–time-resolution measurements of its composition, volatility, and oxidation state. OA and OA precursor gases evolve by becoming increasingly oxidized, less volatile, and more hygroscopic, leading to the formation of oxygenated organic aerosol (OOA), with concentrations comparable to those of sulfate aerosol throughout the Northern Hemisphere. Our model framework captures the dynamic aging behavior observed in both the atmosphere and laboratory: It can serve as a basis for improving parameterizations in regional and global models.

Submicron atmospheric aerosols exert a highly uncertain effect on radiative climate forcing (*1*) and have serious impacts on human health (*2*). Organic aerosol (OA) makes up a large fraction (20 to 90%) of the submicron particulate mass (*3*, *4*). However, OA sources, atmospheric processing, and removal are very uncertain. Primary OA (POA) is directly emitted from fossil fuel combustion, biomass burning, and other sources, but the atmospheric evolution of POA after emission remains poorly characterized (*3*, *4*). Recent results show that secondary OA (SOA), formed by atmospheric oxidation of gas-phase species, accounts for a large fraction of the OA burden (*3*, *5*–*9*). Despite much recent progress in our understanding of SOA formation chemistry (*10*), current "bottom-up" models based on parameterizations of laboratory experiments cannot explain the magnitude and evolution of atmospheric SOA (*5*–*9*). Explicit chemical models are still not able to predict ambient SOA concentrations or degree of oxidation accurately, and they are too complex for large-scale models (*11*). A better understanding of the chemical evolution of OA is required to reduce unacceptable aerosol-related uncertainties in global climate simulations (*12*) and to improve air quality (*13*).

Here we integrate observations and modeling to better characterize the physical and chemical properties and climate effects of OA. Field and laboratory data show that the volatility and oxidation state of organics can be used to build a two-dimensional (2D) modeling framework that maps the evolution of atmospheric OA. The measurements and model reveal OA to be a highly dynamic system, tightly coupled to gas-phase oxidation chemistry. Gas-phase reactions transform OA constituents, and the OA itself is an intermediate, often forming from gas-phase precursors and ultimately returning, in part, to gas-phase products. The framework, though computationally inexpensive, allows an accurate representation of OA in regional and global climate and air-quality models used for policy assessments.

The aerosol mass spectrometer (AMS) detects OA quantitatively by combining thermal vaporization and electron ionization (EI) (*14*). Factor analysis of AMS data (FA-AMS) (*3*, *15*–*17*) demonstrates that AMS data contain sufficient information to differentiate several types of OA and to determine their dry oxygen content (*18*). FA-AMS is based on the total OA mass and avoids the challenges of techniques based on molecular tracers with highly variable tracer:OA ratios (*19*) that may not be stable against atmospheric oxidation (*20*). Figure 1 summarizes FA-AMS results at many locations in the Northern Hemisphere, with typical high-resolution component spectra shown in fig. S1 (*21*). POA from fossil fuel combustion and other urban sources [hydrocarbon-like OA (HOA)] and biomass-burning OA (BBOA) have been identified in multiple studies. However, most OA mass at many locations is oxygenated organic aerosol (OOA) (*3*), characterized by its high oxygen content, with an atomic O:C ratio (an indicator of oxidation state) of 0.25 to ~1 for highly aged OA (*18*). There is strong evidence that most atmospheric OOA is secondary: Increases in OOA are strongly correlated with photochemical activity (*7*, *22*) and other secondary species (*7*, *16*, *17*, *22*), and OOA levels are consistent with SOA estimates using other methods (*13*, *15*).

At many locations, FA-AMS identifies two subtypes of OOA that differ in volatility and O:C (Fig. 1). Volatility and O:C are generally inversely correlated (*16*–*18*, *23*, *24*). Low-volatility OOA (LV-OOA, empirical formula ~$C_8O_{5.5}H_{10}$) is strongly correlated with nonvolatile secondary species such as sulfate and has a high O:C (Fig. 1, inset), consistent with regional, heavily aged OA. Semi-volatile OOA (SV-OOA, empirical formula ~$C_8O_3H_{11}$) has a higher correlation with semivolatile species such as ammonium nitrate and ammonium chloride and has a lower O:C, consistent with less–photochemically aged OA. These two OOA subtypes offer a lumped description of SOA components based on their distinct physicochemical properties. The relative concentrations of the OOA subtypes depend on both ambient temperature and photochemistry. For the three sites with both win-

ter and summer measurements, for example, SV-OOA was observed only during the summer, when the dynamic range in ambient temperature and photochemical conditions is larger.

Recent field and laboratory experiments illustrate the fact that atmospheric oxidation reactions result in the dynamic evolution of OA properties with age. This evolution contrasts sharply with the relatively static nature of sulfate aerosol. In general, atmospheric SV-OOA corresponds to fresh SOA that evolves into LV-OOA with additional photochemical processing. Figure 2, A and B, present data acquired around Mexico City aboard the National Center for Atmospheric Research/National Science Foundation C-130 aircraft during the Megacity Initiative: Local and Global Research Observations (MILAGRO) campaign (*25*). This megacity experiences substantial particulate pollution, including intense SOA formation (*7*, *18*, *22*, *23*, *25*). The aircraft flew over a ground supersite located inside the city (designated as T0) and two sites 30 and 63 km downwind (designated T1 and T2) in the afternoon, corresponding to approximate transport times of 0, 3, and 6 hours from the urban area. In the urban area (T0), SV-OOA was already dominant, consistent with previous observations (*7*), but the fraction of OOA, O:C, and the relative LV-OOA contribution all increased with aging (T0→T1→T2).

A similar transformation has also been observed in the laboratory (Fig. 2, C to F) for various types of OA (*21*). SOA formed from the oxidation of α-pinene becomes more similar to ambient SV-OOA after some aging and then evolves with continued oxidation to become increasingly similar to ambient LV-OOA (Fig. 2C). SOA formation and heterogeneous oxidation from primary diesel emissions, biomass-burning smoke, and the POA surrogate squalane result in strikingly similar transformations (Fig. 2, D to F). The bulk OA spectra in each experiment initially resemble the appropriate source aerosol spectra, but as photochemistry proceeds, their signature is transformed and the laboratory OA spectra become more similar first to that of ambient SV-OOA and then increasingly to that of LV-OOA. These observations, when taken together, indicate that atmospheric oxidation of OA converges toward highly aged LV-OOA regardless of the original OA source, with the original source signature being replaced by that of atmospheric oxidation. This is consistent with the previously reported ubiquity in atmospheric OA of humic-like substances (HULIS), which are complex mixtures of high–molecular-weight polycarboxylic acids that are similar to fulvic acids in soil organic matter (*26*).

An important property of aerosols is hygroscopicity (propensity to absorb water vapor). A more hygroscopic particle of a given size will grow more under humid conditions, scattering more incident light; it will also be more likely to form cloud droplets. Both phenomena strongly influence the radiative forcing of climate through the direct and indirect effects of aerosols (*1*). The dependence of hygroscopicity on particle composition can be represented with the single parameter κ (*27*). Figure 3 shows the relationship between organic O:C and κ for ambient aerosols in urban, forested, and remote locations and also for SOA formed in laboratory chambers from three different precursors (*21*); O:C and κ were determined by AMS and hygroscopicity tandem differential mobility analyzer (HTDMA) (*28*) measurements, respectively. A trend of increasing hygroscopicity with increasing O:C is robust. This strongly suggests that a model must reproduce the evolution of OA shown in Fig. 2 to estimate the variations in OA hygroscopicity, allowing the effects of OA on global climate to be determined more accurately in atmospheric models.

Traditional SOA models are based on the parameterization of smog-chamber experiments, often using a two-product absorptive partitioning scheme (*10*). These models typically do not capture either the amount of SOA or the substantial aging observed in field experiments described above (*7*). Recently, Robinson *et al*. (*29*) proposed an OA model scheme based on lumping species into volatility bins of a basis set (specified as decades in saturation concentration, C^*, at 298 K). This resulted in improved agreement between regional model predictions and ambient measurements. However, simplified lumping schemes based only on volatility cannot represent the broad diversity in physicochemical properties of organic species, such as polarity, solubility, carbon number, and reactivity, and thus may not reproduce the formation rates, properties, or atmospheric fates of OA.

The discussion above underscores the fact that the oxygen content and volatility of OA evolve with photochemical processing. This motivated development of a 2D volatility basis set (2D-VBS) modeling framework using OA volatility (C^*) and oxidation state (here approximated by oxygen content, O:C) as its two basis vectors. Because these two OA properties can be measured in near–real time, this framework can be constrained and directly verified with experimental data, which is an advantage over a previously proposed basis set based on carbon number and polarity (*30*). Moreover, this framework could be used to estimate OA hygroscopicity and would thus introduce an important simplification in atmospheric models.

As shown in Fig. 4, the 2D-VBS (*21*) lumps species with $C^* <\sim 10^7$ μg m^{-3} into bins that are spaced evenly in C^* and O:C space. Each bin includes many organic compounds, spanning only a narrow range of carbon numbers. All constituents are assumed to form a quasi-ideal solution according to standard partitioning theory (*31*). In the atmosphere, only species with $C^* <\sim 10$ μg m^{-3} typically partition substantially into the aerosol (*8*).

Figure 4 shows the location of the OOA factors in the 2D-VBS. Most ambient OA is a mixture of LV-OOA and SV-OOA, with $0.25 < \text{O:C} < 1$ and low C^*. Most primary emissions lie along or near the x axis (low O:C, various C^*). Photochemical reactions cause material to evolve in the 2D space. A key question is, how do primary gas and particle emissions age to become LV-OOA?

The 2D-VBS simulates photochemical aging using a functionalization kernel and a fragmentation kernel, a branching ratio between these two pathways, and a simple representation of differing homogeneous and heterogeneous oxidation by OH (Fig. 4C) (*21*). In the current implementation, the first generation of oxidation is modeled with explicit chemistry but the later generations of oxidation are phenomenological, with param-

[1]Cooperative Institute for Research in the Environmental Sciences and Department of Chemistry and Biochemistry, University of Colorado, Boulder, CO, USA. [2]Aerodyne Research, Billerica, MA, USA. [3]Center for Atmospheric Particle Studies, Carnegie Mellon University, Pittsburgh, PA, USA. [4]Laboratory of Atmospheric Chemistry, Paul Scherrer Institut, Villigen, Switzerland, [5]Atmospheric Sciences Research Center, State University of New York, Albany, NY, USA. [6]Department of Environmental Toxicology, University of California, Davis, CA, USA. [7]Department of Civil and Environmental Engineering, Massachusetts Institute of Technology, Cambridge, MA, USA. [8]Department of Atmospheric and Oceanic Science, University of Colorado, Boulder, CO, USA. [9]School of Earth, Atmospheric, and Environmental Science, University of Manchester, Oxford Road, Manchester, UK. [10]National Centre for Atmospheric Science, University of Manchester, Oxford Road, Manchester, UK. [11]Chemical Sciences Division, Lawrence Berkeley National Laboratory, Berkeley, CA, USA. [12]Empa, Laboratory for Air Pollution/Environmental Technology, Dübendorf, Switzerland. [13]Department of Physics, University of Kuopio, Kuopio, Finland. [14]Finnish Meteorological Institute, Helsinki, Finland. [15]Department of Physics, University of Helsinki, Helsinki, Finland. [16]Department of Applied Environmental Science, Stockholm University, Stockholm, Sweden. [17]Department of Atmospheric Sciences, Texas A&M University, College Station, TX, USA. [18]Research Center for Advanced Science and Technology, University of Tokyo, Tokyo, Japan. [19]Department of Particle Chemistry, Max Planck Institute for Chemistry, Mainz, Germany. [20]Institute for Atmospheric Physics, Johannes Gutenberg University, Mainz, Germany. [21]Empa, Laboratory for Internal Combustion Engines, Dübendorf, Switzerland. [22]Centro de Investigaciones Quimicas, Universidad Autonoma del Estado de Morelos, Cuernavaca, Mexico. [23]Climate Change Research Center, University of New Hampshire, Durham, NH, USA. [24]Department of Civil and Environmental Engineering, Rice University, Houston, TX, USA. [25]Asian Environmental Research Group, National Institute for Environmental Studies, Tsukuba, Japan. [26]Sanyu Plant Service, Sagamihara, Japan. [27]Key Laboratory for Atmospheric Chemistry, Chinese Academy of Meteorological Sciences, Beijing, China. [28]Atmospheric Chemistry Division, National Center for Atmospheric Research, Boulder, CO, USA. [29]Tofwerk, Thun, Switzerland. [30]Earth Science Research Laboratory, National Oceanic and Atmospheric Administration, Boulder, CO, USA.

*To whom correspondence should be addressed. E-mail: jose.jimenez@colorado.edu (J.L.J.); andre.prevot@psi.ch (A.S.H.P.)

†Present address: Swiss Federal Institute of Technology, Zurich, Switzerland.

‡Present address: Institute for Resources, Environment and Sustainability, University of British Columbia, Vancouver, Canada.

§Present address: CERN, Geneva, Switzerland.

||Present address: Pacific Northwest National Laboratory, Richland, WA, USA.

¶Present address: Climate Program Office, National Oceanic and Atmospheric Administration, Silver Spring, MD, USA.

#Present address: Department of Biogeochemistry, Max Planck Institute for Chemistry, Mainz, Germany.

††Present address: Environ International, Groton, MA, USA.

‡‡Present address: Tokyo Metropolitan Research Institute for Environmental Protection, Tokyo, Japan.

§§Present address: Institute of Symbiotic Science and Technology, Tokyo University of Agriculture and Technology, Tokyo, Japan.

|| ||Present address: Shoreline Science Research, Tokyo, Japan.

¶¶Present address: Department of Particle Chemistry, Max Planck Institute for Chemistry, Mainz, Germany.

eters consistent with our current understanding of atmospheric chemistry. It can be applied to material produced from any precursor.

To test whether the model can reproduce the transformations of atmospheric OA shown in Fig. 2, the simulated formation and aging chemistry of α-pinene SOA (and the attendant vapors) are shown in Fig. 4. The full (vapor and particle) first-generation distribution from the α-pinene + O_3 reaction (derived from chamber data) is shown with blue contours in Fig. 4A, having $1 < C^* < 10^7$ μg m^{-3} and 0.1 < O:C < 0.4. Lower-volatility products to the upper left of the blue contours condense to form SOA. The reaction of the first-generation particle and vapor distribution with OH is modeled with functionalization reactions that generate products that are roughly within the limits indicated by the red dashed lines in Fig. 4A. The predicted condensed-phase products after 1.5 lifetimes of OH oxidation are shown with purple contours in Fig. 4A and the yellow star in Fig. 4, A and B. The model predicts a tripling of SOA mass by the end of the second generation of oxidation. This increase is also accompanied by an increase in O:C, shown in Fig. 4B, and a drop in average C^* of the aerosol. The predictions in Fig. 4 are consistent with observations of *cis*-pinonic acid, a typical first-generation reaction product, and of its OH oxidation product α,α-dimethyltricarballylic acid (*8*). Moreover, the simulation results reproduce the SV-OOA–to–LV-OOA transformation observed in the laboratory experiments on α-pinene SOA aging (Fig. 2C).

The model predicts very similar outcomes for the aging of other SOA precursors, including the evaporated diesel and biomass-burning smoke shown in Fig. 2, E and F. Most of the aging in these simulations occurs via gas-phase oxidation of semivolatile vapors. OOA formation occurs mainly via condensation of the less volatile products of these aging reactions on accumulation-mode particles, where OOA principally resides (*15*). However, in all of these cases, the majority of the oxidation products in the model are higher-volatility gases. Although the current implementation of the framework considers aging only by reactions with OH, other aging mechanisms, such as oligomerization or the addition of hydrated glyoxal to a semivolatile organic in the condensed phase (*32*), could be incorporated into the framework. These mechanisms represent other means of substantially increasing O:C while reducing C^* by several decades.

OA is dynamic and continually evolves in the atmosphere; this evolution strongly influences the effects of particulate matter on climate and air quality. The complex evolution of OA contrasts with the simpler behavior of sulfate, which is irreversibly oxidized and condensed. Current modeling frameworks for OA are constructed in an analogous way to those for sulfate, with either no aging or one-step oxidation. Here we have presented a unifying framework describing the atmospheric evolution of OA, which is directly connected to worldwide observations and experimentally verifiable and can be used to evaluate and form the basis of practical phenomenological modeling

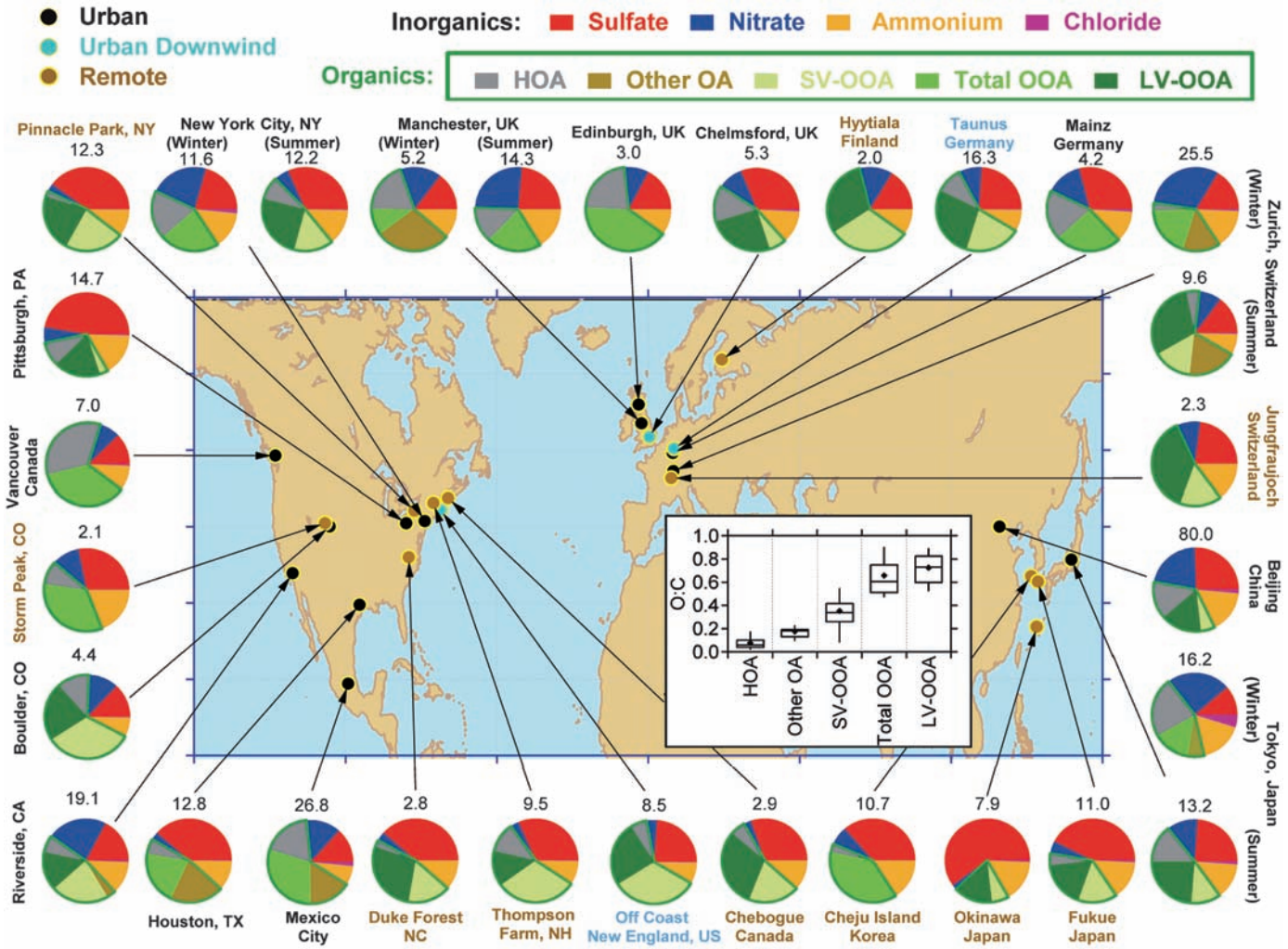

Fig. 1. Total mass concentration (in micrograms per cubic meter) and mass fractions of nonrefractory inorganic species and organic components in submicrometer aerosols measured with the AMS at multiple surface locations in the Northern Hemisphere (*21*). The organic components were obtained with FA-AMS methods (*3*, *15*–*17*). In some studies, the FA-AMS methods identified one OOA factor, whereas in other locations, two types, SV-OOA and LV-OOA, were identified. HOA is a surrogate for urban primary OA, and Other OA includes primary OAs other than HOA that have been identified in several studies, including BBOA. (Inset) Distributions of O:C for the OA components identified at the different sites, calculated according to (*18*).

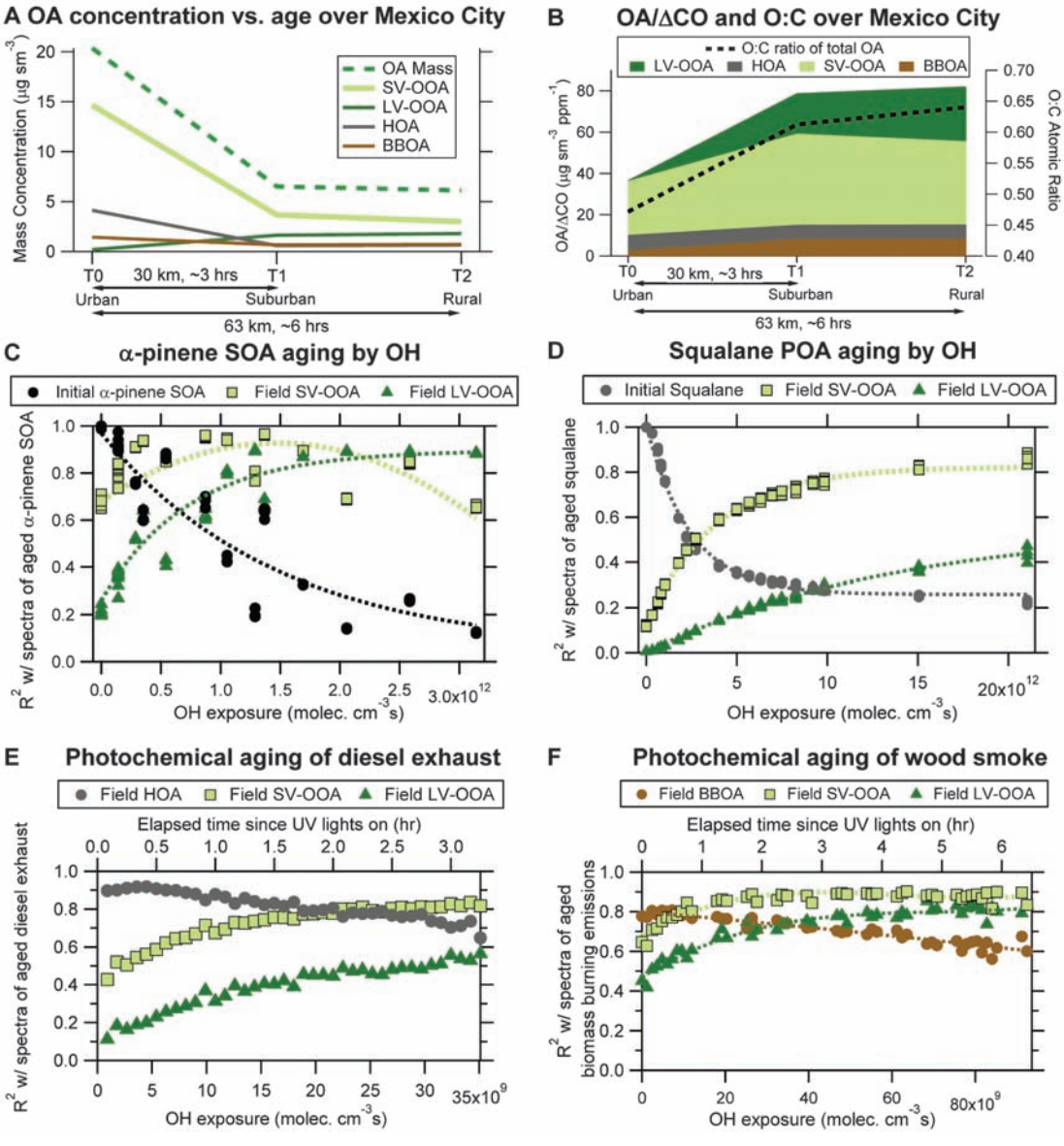

Fig. 2. Field and laboratory data of OA evolution with photochemical aging. (**A** and **B**) Atmospheric aging of OA above the T0→T1→T2 sites in and around Mexico City (corresponding to approximate transport times of 0, 3, and 6 hours from the urban area) as measured from the C-130 aircraft during the MILAGRO field experiment. OA/ΔCO, where ΔCO is the measured CO minus a Northern Hemispheric background of 100 parts per billion by volume, is plotted in (B) to correct for dilution of the air mass. Biomass burning was suppressed by rain during this period. (**C** to **F**) Evolution of OA composition during photochemical aging in laboratory reaction chambers of (C) α-pinene SOA, (D) squalane (a liquid hydrocarbon used as a surrogate for reduced primary OA), (E) diesel exhaust, and (F) biomass-burning smoke. In (C) to (F), the increased degree of oxidation and similarity to ambient OOA spectra are indicated by the Pearson correlation coefficients (R^2) between the evolving total OA spectra in each experiment and the SV-OOA and LV-OOA spectra derived from the Mexico City field data set. The similarity to the initial source spectra decreases in all cases: For α-pinene and squalane, the evolving OA is compared to the original OA, whereas for diesel exhaust and wood smoke, it is compared with ambient HOA and BBOA from Mexico City. Dashed lines are included to guide the eye.

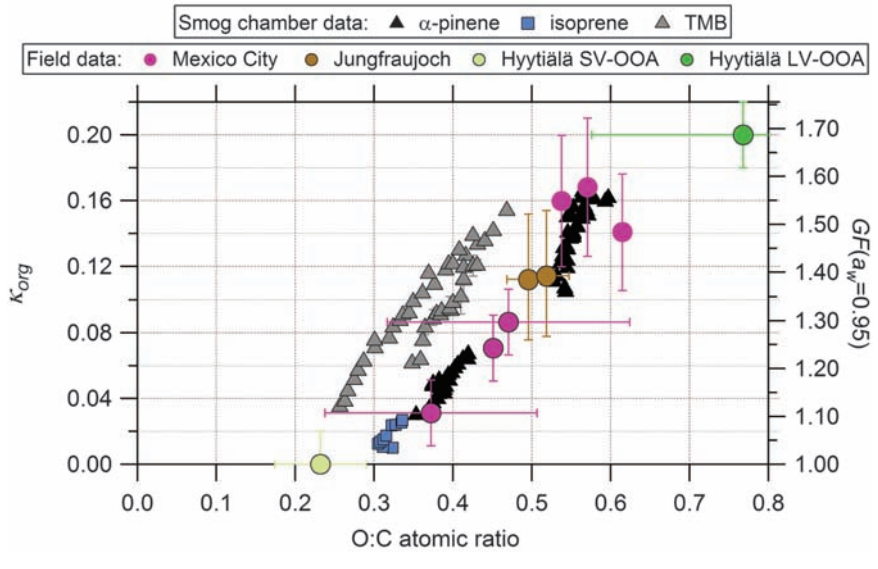

Fig. 3. Relationship between O:C and hygroscopicity (κ, or equivalently the particle growth factor at 95% relative humidity) of OA for several field data sets (a high-altitude site at Jungfraujoch, Switzerland; above Mexico City, a polluted megacity; and at the forested site of Hyytiälä, Finland) and for laboratory smog chamber SOA (*21*). TMB, trimethylbenzene. Error bars represent the uncertainties in O:C and κ_{org} (org, organic) and are shown for only a few data points to reduce visual clutter. *GF*, growth factor; a_w, water activity.

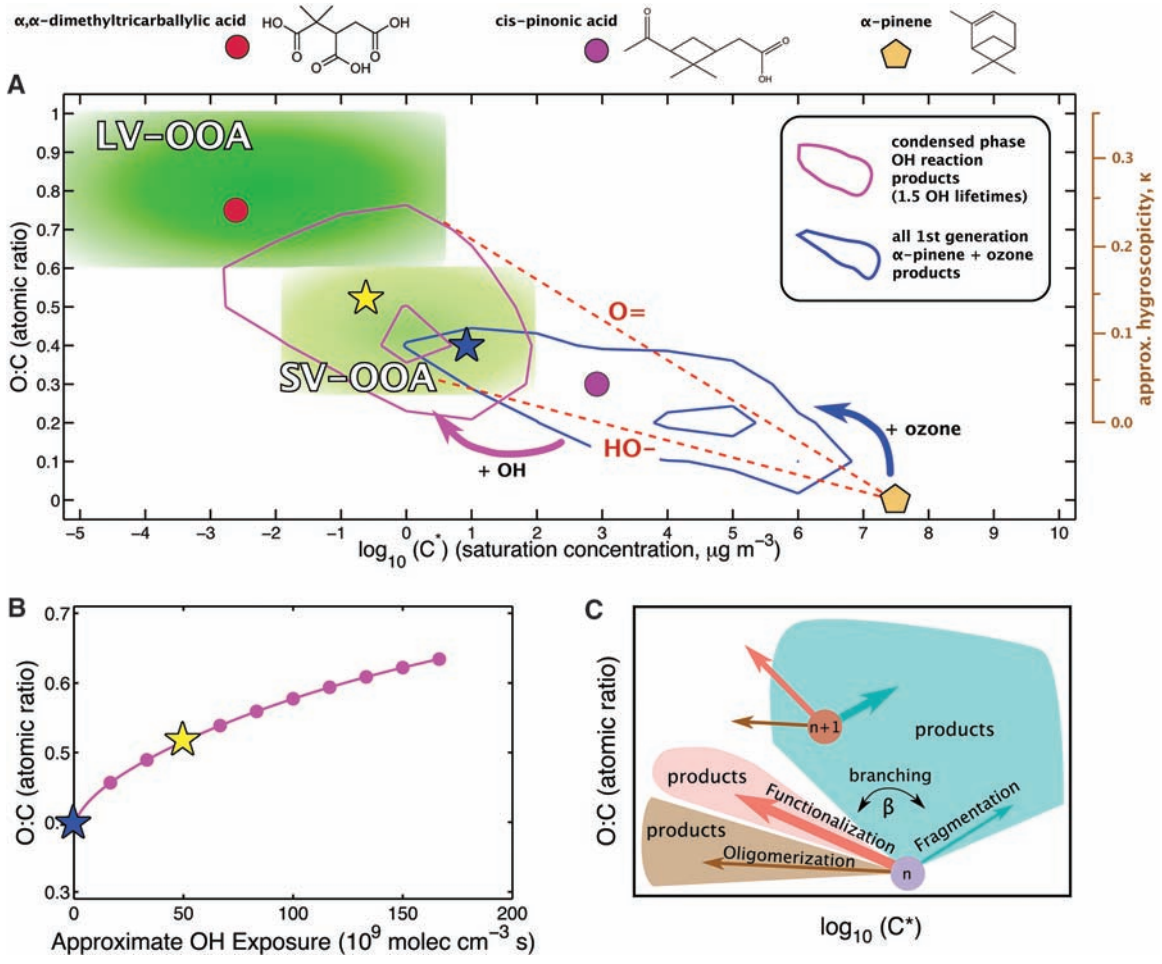

Fig. 4. (**A**) 2D framework for OA aging. The *x* axis is volatility ($\log_{10}$ of C^* at 298 K). The *y* axis is oxidation state, approximated by O:C. The secondary *y* axis shows the approximate κ of α-pinene SOA from Fig. 3. Compounds with $C^* \leq C_{OA}$ (the organic aerosol concentration, typically 1 to 10 μg m^{-3}) favor the condensed phase. Those with $C^* > C_{OA}$ favor the gas phase. The OOA factors described in Figs. 1 to 3 fall in this 2D space as shown by the green areas, with LV-OOA being less volatile and more oxidized than SV-OOA. We modeled the initial oxidation of common precursors with explicit chemistry, but later-generation oxidation applies to material produced from any precursor. α-pinene (brown pentagon) is an example. All products from the α-pinene + ozone reaction, modeled explicitly, are distributed according to the blue contours; the material at low C^* and high O:C forms SOA (with mean properties indicated by the blue star). Typical effects of adding (=O) and (–OH) functionality to a C_{10} backbone are shown with red dashed lines, and a common first-generation product, *cis*-pinonic acid, is shown with a magenta dot. After forming α-pinene SOA explicitly, we modeled subsequent aging reactions with OH within the 2D-VBS. A representative second-generation product, a C_8 triacid, is shown with a crimson dot within the LV-OOA range. Modeled condensed-phase products after 1.5 lifetimes of OH oxidation are shown with purple contours. The mass-weighted average is indicated by the yellow star. This simulation reproduces a substantial shift toward ambient OOA characteristics, indicated by the shift between the blue and yellow stars. (**B**) Evolution of condensed-phase O:C versus approximate OH exposure for simulated aging (similar to Fig. 2C). The blue and yellow stars for organic aerosol in (A) are shown. (**C**) Oxidation can occur in the gas or condensed phase, and reactions transform material as shown (*21*). Reactions form three categories: fragmentation, functionalization, or oligomerization, based on whether the carbon number decreases, stays the same, or increases. Here we model the first two pathways. The branching ratio (β) between these pathways is critical. Functionalization will reduce volatility considerably, whereas fragmentation can generate more-volatile species, which are less likely to partition to the OA.

approaches. The combination of measurements and the modeling framework implies that most OA is an intermediate state of organic material, between primary emissions of reduced species and highly oxidized volatile products (CO and CO_2). Future models, inventories, and measurements will almost certainly need to account for the dynamic sources and sinks of OA to accurately predict regional and global OA distributions and properties and thus the associated health and climate effects.

References and Notes

1. P. Forster *et al.*, in S. Solomon *et al., IPCC 4th Assessment Report* (Cambridge Univ. Press, Cambridge, 2007), chap. 2.
2. A. Nel, *Science* **308**, 804 (2005).
3. Q. Zhang *et al.*, *Geophys. Res. Lett.* **34**, L13801 (2007).
4. D. M. Murphy *et al.*, *J. Geophys. Res.* **111**, D23S32 (2006).
5. C. L. Heald *et al.*, *Geophys. Res. Lett.* **32**, L18809 (2005).
6. J. A. de Gouw *et al.*, *J. Geophys. Res.* **110**, D16305 (2005).
7. R. Volkamer *et al.*, *Geophys. Res. Lett.* **33**, L17811 (2006).
8. M. Hallquist *et al.*, *Atmos. Chem. Phys.* **9**, 5155 (2009).
9. A. H. Goldstein, I. E. Galbally, *Environ. Sci. Technol.* **41**, 1514 (2007).
10. J. H. Kroll, J. H. Seinfeld, *Atmos. Environ.* **42**, 3593 (2008).
11. D. Johnson *et al.*, *Atmos. Chem. Phys.* **6**, 403 (2006).
12. J. T. Kiehl, *Geophys. Res. Lett.* **34**, L22710 (2007).
13. K. S. Docherty *et al.*, *Environ. Sci. Technol.* **42**, 7655 (2008).
14. M. R. Canagaratna *et al.*, *Mass Spectrom. Rev.* **26**, 185 (2007).
15. Q. Zhang, D. R. Worsnop, M. R. Canagaratna, J. L. Jimenez, *Atmos. Chem. Phys.* **5**, 3289 (2005).
16. V. A. Lanz *et al.*, *Atmos. Chem. Phys.* **7**, 1503 (2007).
17. I. M. Ulbrich, M. R. Canagaratna, Q. Zhang, D. R. Worsnop, J. L. Jimenez, *Atmos. Chem. Phys.* **9**, 2891 (2009).
18. A. C. Aiken *et al.*, *Environ. Sci. Technol.* **42**, 4478 (2008).
19. R. Subramanian, N. M. Donahue, A. Bernando-Bricker, W. F. Rogge, A. L. Robinson, *Atmos. Environ.* **40**, 8002 (2006).
20. E. A. Weitkamp, K. E. Huff Hartz, A. M. Sage, N. M. Donahue, A. L. Robinson, *Environ. Sci. Technol.* **42**, 5177 (2008).
21. Materials and methods are available as supporting material on *Science* Online.
22. S. C. Herndon *et al.*, *Geophys. Res. Lett.* **35**, L15804 (2008).
23. J. A. Huffman *et al.*, *Atmos. Chem. Phys.* **9**, 7161 (2009).
24. A. P. Grieshop, N. M. Donahue, A. L. Robinson, *Atmos. Chem. Phys.* **9**, 2227 (2009).
25. P. F. DeCarlo *et al.*, *Atmos. Chem. Phys.* **8**, 4027 (2008).
26. S. Fuzzi *et al.*, *Geophys. Res. Lett.* **28**, 4079 (2001).
27. M. D. Petters, S. M. Kreidenweis, *Atmos. Chem. Phys.* **7**, 1961 (2007).
28. D. J. Rader, P. H. McMurry, *J. Aerosol Sci.* **17**, 771 (1986).
29. A. L. Robinson *et al.*, *Science* **315**, 1259 (2007).
30. J. F. Pankow, K. C. Barsanti, *Atmos. Environ.* **43**, 2829 (2009).
31. J. F. Pankow, *Atmos. Environ.* **28**, 189 (1994).
32. R. Volkamer *et al.*, *Geophys. Res. Lett.* **34**, L19807 (2007).

33. This work was supported by NSF's Atmospheric Chemistry Program, the Environmental Protection Agency's Science to Achieve Results program, the Department of Energy's Office of Biological and Environmental Research/Atmospheric Science Program, the National Oceanic and Atmospheric Administration Office of Global Programs, the Swiss NSF, EUROCHAMP, and other funding agencies listed in table S1.

Supporting Online Material

www.sciencemag.org/cgi/content/full/326/5959/1525/DC1
Materials and Methods
Figs. S1 to S3
Tables S1 to S4
References

10 August 2009; accepted 6 November 2009
10.1126/science.1180353

Science

Evolution of Organic Aerosols in the Atmosphere

J. L. Jimenez, M. R. Canagaratna, N. M. Donahue, A. S. H. Prevot, Q. Zhang, J. H. Kroll, P. F. DeCarlo, J. D. Allan, H. Coe, N. L. Ng, A. C. Aiken, K. S. Docherty, I. M. Ulbrich, A. P. Grieshop, A. L. Robinson, J. Duplissy, J. D. Smith, K. R. Wilson, V. A. Lanz, C. Hueglin, Y. L. Sun, J. Tian, A. Laaksonen, T. Raatikainen, J. Rautiainen, P. Vaattovaara, M. Ehn, M. Kulmala, J. M. Tomlinson, D. R. Collins, M. J. Cubison, E., J. Dunlea, J. A. Huffman, T. B. Onasch, M. R. Alfarra, P. I. Williams, K. Bower, Y. Kondo, J. Schneider, F. Drewnick, S. Borrmann, S. Weimer, K. Demerjian, D. Salcedo, L. Cottrell, R. Griffin, A. Takami, T. Miyoshi, S. Hatakeyama, A. Shimono, J. Y Sun, Y. M. Zhang, K. Dzepina, J. R. Kimmel, D. Sueper, J. T. Jayne, S. C. Herndon, A. M. Trimborn, L. R. Williams, E. C. Wood, A. M. Middlebrook, C. E. Kolb, U. Baltensperger and D. R. Worsnop

Science **326** (5959), 1525-1529.
DOI: 10.1126/science.1180353

Framework for Change

Organic aerosols make up 20 to 90% of the particulate mass of the troposphere and are important factors in both climate and human heath. However, their sources and removal pathways are very uncertain, and their atmospheric evolution is poorly characterized. **Jimenez *et al.*** (p. 1525; see the Perspective by **Andreae**) present an integrated framework of organic aerosol compositional evolution in the atmosphere, based on model results and field and laboratory data that simulate the dynamic aging behavior of organic aerosols. Particles become more oxidized, more hygroscopic, and less volatile with age, as they become oxygenated organic aerosols. These results should lead to better predictions of climate and air quality.